DOI: 10.1002/adsc.201601317

Advanced Synthesis & Catalysis

Regio- and Stereospecific *O*-Glycosylation of Phenolic Compounds Catalyzed by a Fungal Glycosyltransferase from *Mucor hiemalis*

Jin Feng,[+a,b,c] Peng Zhang,[+a,d] Yinglu Cui,[c] Kai Li,[b] Xue Qiao,[b] Ying-Tao Zhang,[b] Shu-Ming Li,[e] Russell J. Cox,[f] Bian Wu,[c] Min Ye,[b,*] and Wen-Bing Yin[a,d,*]

[a] State Key Laboratory of Mycology, Institute of Microbiology, Chinese Academy of Sciences, 100101 Beijing, People's Republic of China
Fax: (+86)-10-6480-6170; phone: (+86)-10-6480-6170; e-mail: yinwb@im.ac.cn
[b] State Key Laboratory of Natural and Biomimetic Drugs, School of Pharmaceutical Sciences, Peking University, 100191 Beijing, People's Republic of China
Fax: (+86)-10-8280-2024; phone: (+86)-10-8280-2024; e-mail: yemin@bjmu.edu.cn
[c] State Key Laboratory of Transducer Technology, Chinese Academy of Sciences, 100101 Beijing, People's Republic of China
[d] Savaid Medical School, University of Chinese Academy of Sciences, 100049 Beijing, People's Republic of China
[e] Philipps-Universität Marburg, Institut für Pharmazeutische Biologie und Biotechnologie, Robert-Koch-Strasse 4, 35037 Marburg, Germany
[f] Institute for Organic Chemistry, Leibniz Universität Hannover and Centre of Biomolecular Drug Research (BMWZ), Schneiderberg 1B, 30167 Hannover, Germany
[+] These authors contributed equally to this work.

Received: November 29, 2016; Revised: January 4, 2017; Published online: ■■ ▮▮, 0000

Supporting information for this article is available under http://dx.doi.org/10.1002/adsc.201601317.

Abstract: Glycosylated small molecules are often bioactive and obtained mainly *via* microbial biotransformation especially by fungi. However, no responsible glycosylation gene/enzyme has yet been uncovered in a filamentous fungus. We report here the first identification of a phenolic glycosyltransferase MhGT1 from *Mucor hiemalis*. The substrate promiscuity of the new phenolic *O*-glycosyltransferase was explored by using phenols from Traditional Chinese Medicinal herbs as substrates. MhGT1 exhibited robust capabilities for the regio- and stereospecific *O*-glycosylation of 72 structurally diverse drug-like scaffolds and sterols with uridine diphosphate (UDP) glucose as a sugar donor. Unprecedentedly, MhGT1 showed higher regiospecificities and activities for prenylated phenols than for their non-prenylated analogues. Computational modelling of MhGT1 uncovered a truncated *N*-terminal domain of the enzyme consisting of hydrophobic and charged amino acid residues which contributed to the broad substrate scope and regiospecificity towards prenylated compounds. Our findings expand the ways to obtain new glycosyltransferases and also effectively apply the enzymatic approach to obtain glycosylated compounds in drug discovery.

Keywords: computational modelling; enzymatic catalysis; glycosyltransferases; *Mucor hiemalis*; substrate promiscuity

Introduction

Glycosylation of natural products catalyzed by glycosyltransferases (GTs) plays a central role in drug discovery and development.[1–4] Therefore, many strategies have been developed to obtain glycosylated small molecules.[5] One of the most commonly used approaches is biotransformation with various microbes such as *Aspergillus*, *Beauveria*, *Cunninghamella* and *Penicillium* spp. which display excellent conversion yields.[6,7] For example, *B. bassiana* AM278 converted 8-prenylnaringenin into the corresponding 7-*O*-β-D-(4‴-*O*-methyl)-glucopyranoside in 34.0% yield.[8] *Cunninghamella* sp. converted silybin into the phase II microbial metabolites 2,3-dehydrosilybin 3-*O*-β-D-glucoside, silybin 7-sulfate and 2,3-dehydrosily-

bin 7-sulfate which retained antioxidant activity.[9] The use of purified (and often engineered) GTs is also effective[10,11] because enzymes often exhibit higher efficiency and controllability than whole-cell systems.[3] For example, the Thorson group characterized bacterial GTs, engineered them for production of novel glycosylated natural products and studied their catalytic promiscuities.[10,12,13] Furthermore, plant GTs have been identified for the *O*/*C*-glycosylation of small molecules such as UGT73AE1 from *Carthamus tinctorius* and *C*-GT from *Mangifera indi*ca.[14,15] To date, a number of GTs have been characterized from bacteria,[13] yeasts and plants, but not from filamentous fungi.[15] Moreover, the characterized GTs showed lower substrate scope. This is in sharp contrast to the reported predominant production of glycosylated compounds by successful fungal biotransformations. This discrepancy encouraged us to search for new fungal natural-product GTs and probe their functions.

A number of fungal strains including *A. nidulans*, *Pestalotiopsis fici* as well as *Mucor hiemalis* were therefore selected for this purpose in our previous work. *M. hiemalis* was found to exhibit excellent capability for glycosylation of prenylated phenolic compounds.[16] Thus, we reasoned that *M. hiemalis* would be a good source for new fungal GTs. In this study, we present the discovery of the first phenolic GT from the filamentous fungus *M. hiemalis*. It shows the robust capability to catalyze 72 structurally diverse drug-like substrates from a 93 compound library. Computational modelling shows a truncated *N*-terminal domain containing a mixture of hydrophobic and charged residues in MhGT1 which reveals the large active cavity of the enzyme. Therefore, MhGT1 shows broader substrate scope and regiospecificities to prenylated compounds. Finally, we isolated and elucidated the structures of 10 novel glycosylated small molecules. Seven of them have both prenyl and glycosyl moieties which are structurally very rare in nature.

Results and Discussion

Discovery and Characterization of a New GT from *M. hiemalis*

To find the novel GT and probe our hypothesis, we performed transcriptome analysis *via M. hiemalis* transformation with/without feeding of compound glycyrol **1** to shed light on the expressions of GTs. Firstly, we investigated the time-course of glycosylation by feeding glycyrol **1** to *M. hiemalis* (Figure 1) and subsequent analysis of its glycosylation. LC-MS analysis revealed the decrease of the substrate peak and appearance of a new peak at 16.1 min. Almost total conversion was observed after 24 h (Figure 1A). $[M-H]^-$

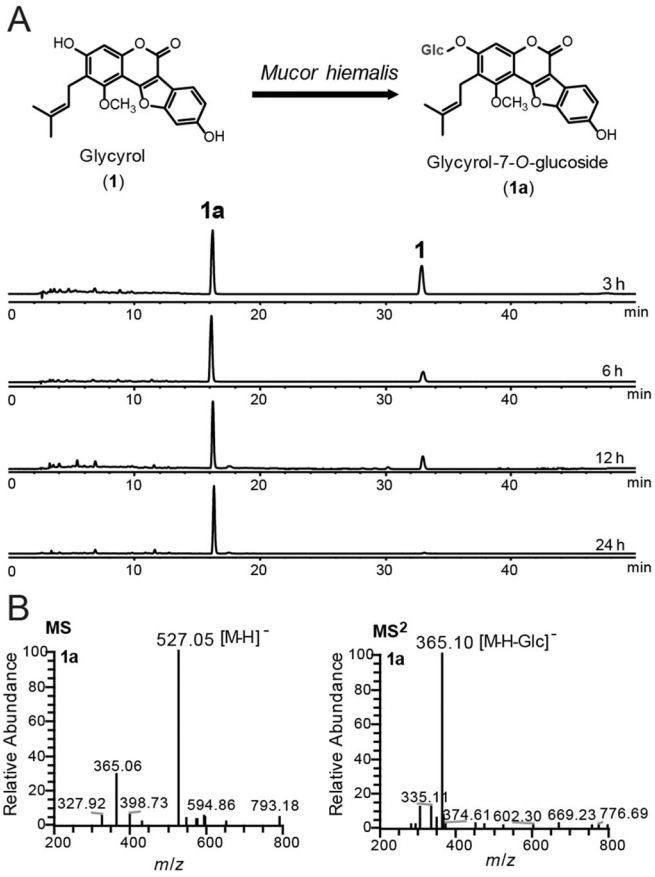

Figure 1. Biotransformation of glycyrol **1** by *M. hiemalis*. (A) HPLC analysis of transformed **1** in time-course reaction. **1** was fed to *M. hiemalis* and the cultures were collected in 3 h, 6 h, 12 h and 24 h for analysis. (B) MS analysis of substrate and transformed product.

ion of the product peak at $m/z = 527$, which is 162 amu larger than that of glycyrol, suggested the presence of a glucose or analogue residue in the product and proved unequivocally the glycosylation of the substrate (Figure 1B). This result confirmed the ability of *M. hiemalis* for glycosylation.

Next, total RNAs were extracted from *M. hiemalis* during the GT reaction in the presence and absence of **1** for RNA-seq analysis. RNA-seq data analyses showed 140 differentially expressed genes with putative GT functions (Supporting Information, pages 62 and 63). In order to narrow down the target gene, we carried out alignments of predicted GTs from *M. hiemalis* (Supporting Information, pages 62 and 63) with known ones from bacteria and plants. Using this approach, we targeted a gene, named *MhGT1* (GenBank Accession Number: KU885980), with very low identities on the amino acid level to bacterial GTs (Supporting Information, Figure S1). This gene shared an identity of 29% with *Bacillus cereus BcGT-1*.[17] *MhGT1* was cloned from cDNA and fused with a maltose-binding protein (MBP) tag for expression in *E.*

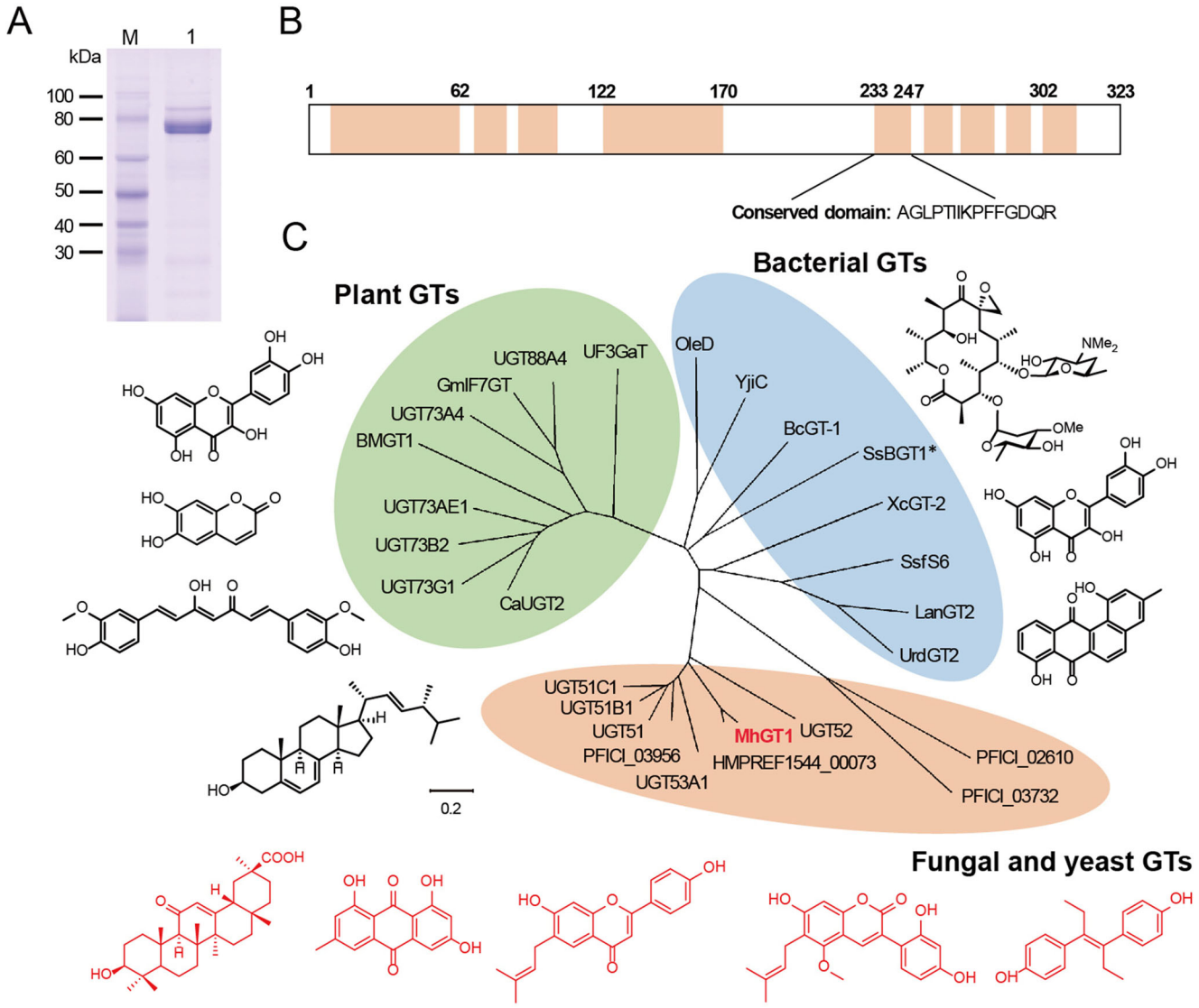

Figure 2. Characterization and phylogenetic analysis of recombinant MhGT1. (A) SDS-PAGE of the recombinant MhGT1 fused with MBP tag. M: protein maker; 1: recombinant MhGT1 (predicted MW: 81.1 kDa). (B) Fragment distribution of recombinant MhGT1 detected by LC-MS/MS. The amino acid region in 233–247 belongs to the conserved domain of glycosyltransferases. (C) Phylogenetic analysis of MhGT1 and 26 glycosyltransferases from plants, bacteria and fungi. The major substrate types accepted by plant UDP-glycosyltransferases are flavonoids, coumarins, curcumin, and other phenolic compounds. Bacterial glycosyltransferases mainly catalyze glucosylation of flavonoids, oleandomycin, and the aglycones of landomycin A and urdamycin A. MhGT1 catalyzes glucosylation of phenolic compounds, steroids and terpenoids.

coli. MhGT1 protein was purified to near homogeneity (Experimental Section) and analyzed on SDS-PAGE (Figure 2A). LC-MS/MS analysis confirmed that MhGT1 is the target protein with the MBP tag sequence (score: 2076.14, coverage: 64.25%) and a GT conserved region PTIIKPFFGDQ (score: 1167.02, coverage: 69.44%) as expected (Figure 2B).[18]

MhGT1 was then incubated *in vitro* with glycyrol **1** and UDP-glucose. LC-MS analysis confirmed the same $[M-H]^-$ ion at $m/z=527$ of the enzyme product **1a** as that of the product obtained from biotransformation (Figure 1B). The structure of the product was elucidated by HR-ESI-MS, ^{1}H NMR, ^{13}C NMR and HMBC analyses (Supporting Information, Table S1, Figures S12–S14) and proven to be the expected *O*-glycosylated derivative **1a**. This result provided evidence for the function of MhGT1 as the GT responsible for the whole-cell activity.

Regarding the very low similarities of MhGT1 with known bacterial or plant GTs, we reasoned that it belongs to a new enzyme group. Phylogenetic analysis did indeed reveal that MhGT1 clustered to an individual clade with other fungal and yeast GTs including the yeast GTs UGT51, UGT51B1, UGT51C1 which have been previously characterized as sterol GTs.[19]

In comparison, bacterial GTs function as flavonoid or polyketide GTs and plant GTs function as flavone GTs (Figure 2C).[20,21] No functions have yet been proven for other fungal GTs.

Biochemical Characterization of MhGT1

To study the biochemical properties and dynamic parameters, the recombinant MhGT1 was then purified in a large-scale culture (Experimental Section). By using glycycoumarin **2** and UDP-glucose as substrates, the MhGT1 reaction was found to have an optimized working temperature at 30–40 °C, pH at 8.0–9.0 and is enhanced by Ca^{2+}, Mg^{2+} and Ba^{2+} ions up to two-fold (Supporting Information, Figure S2). Using compounds **3** and UDP-glucose as substrates, MhGT1 catalyzed the formation of two *O*-glycosylated products **3a** and **3b**. In comparison, the prenylated substrate **4** was converted to the sole product **4a** (Figure 3, and Supporting Information, Table S1). The structures of the products were elucidated by HR-ESI-MS, ^{1}H NMR, ^{13}C NMR and HMBC analyses (Supporting Information, Table S1, Figures S15–S22). K_m values of MhGT1 toward **2**, **4**, **13** and **14** were found to be 32.9 μM, 16.4 μM, 8.0 μM and 44.2 μM (Supporting Information, Figure S3), respectively, and the corresponding K_{cat} values for **2**, **4**, **13** and **14** were 1.85×10^{-3} s^{-1}, 1.15×10^{-3} s^{-1}, 0.68×10^{-3} s^{-1} and 2.42×10^{-3} s^{-1}, respectively. In comparison, K_m values of plant *Catharanthus roseus* UDP-glucosyltransferase CaUGT2 were 19.0 μM for its substrate curcumin, 660–1120 μM for other substrates like esculetin, scopoletin, *p*-nitrophenol and vanillin, and K_{cat} values of ASP OleD were 0.020 S^{-1}, 0.107 S^{-1}, and 0.096 S^{-1} for substrates phenol, thiophenol and aniline, respectively.[22,23]

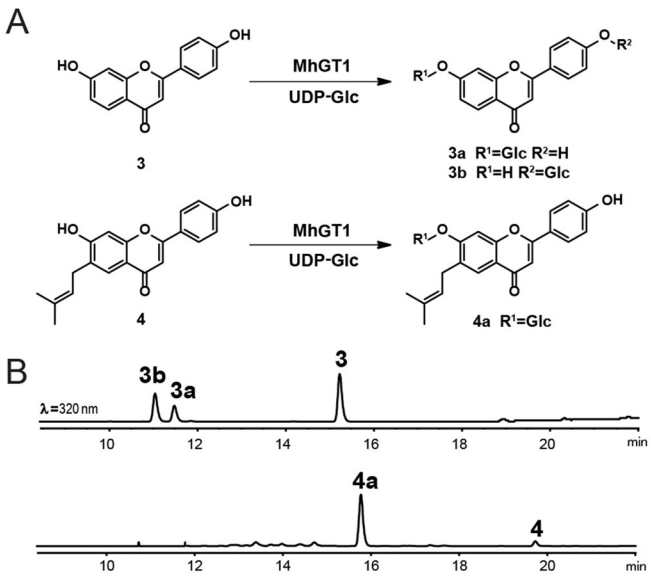

Figure 3. *O*-Glycosylation of **3** and **4** catalyzed by MhGT1. (A) The reactions catalyzed by the purified MhGT1. (B) HPLC chromatograms of the reaction mixtures of **3** and **4** and the enzymatic products **3a**, **3b** and **4a**. The HPLC conditions are provided in the Experimental Section.

MhGT1 Exhibited Broad Substrate Specificity

To explore the substrate promiscuity and probe the synthetic biological utility of this novel GT *in vitro*, an acceptor library of 93 representative natural and unnatural compounds with structural diversity was assessed with UDP-glucose as sugar donor. The library included 4 coumarins (**1**, **2**, **13**, **60**), 56 flavonoids (**3**–**12**, **14**–**59**), 3 coumarones (**61**–**63**), 1 anthraquione (**64**), 3 steroids (**65**–**67**), 5 terpenoids (**68**, **87**–**90**), 3 flavonoid glucosides (**73**–**75**), 1 tyrosine (**77**), 7 alkaloids (**78**–**84**), 1 tanshinone (**85**), 1 lignan (**86**), 3 antibiotics (**91**–**93**) and 5 simple phenols (**69**–**72**, **76**) (Supporting Information, Figures S4 and S5). The reactions were evaluated initially by LC-MS analysis. In some cases (like, for example, **6** and **7**, Supporitng Information, Figure S4) as many as six different products were observed although most substrates gave only 1, 2 or 3 products. These correspond to different regioisomeric species and to the addition of multiple glycosides. The products are labelled **a**–**f** and represented by different colours in Figure 4 and Figure 6.

The results revealed that this enzyme was sufficiently flexible to *O*-glycosylate 72 of the 93 tested substrates (77%) (Figure 4, and Supporting Information, Table S1). All the glycosylated products were confirmed by LC-MS analysis (Supporting Information, Table S1). These include 4 coumarins (**1**, **2**, **13**, **60**), 56 flavonoids (**3**–**12**, **14**–**59**), 3 coumarones (**61**–**63**), 1 anthraquione (**64**), 3 steroids (**65**–**67**), 1 terpenoids (**68**) and 4 other types of phenolic compounds (**69**–**72**) (Supporting Information, Figure S4 and Table S1). 21 compounds including the alkaloids **78**–**84** and antibiotics **91**–**93** were not accepted by MhGT1 (Supporting Information, Figure S5). In comparison with oleandomycin GT OleD from *Streptomyces antibioticus*, engineered OleD variants greatly enhanced the rates of substrate acceptance with 52% (71 of the 135 library members)[23] which is much lower than MhGT1 with 77%. To the best of our knowledge, the substrate specificity of MhGT1 as an *O*-glycosyl transferase is the most diverse known to date.[14,23,24]

Interestingly, MhGT1 also exhibited *O*-glycosylation activity for **2**, when UDP-galactose was used as an alternative sugar donor. A product peak was detected at the retention time 15.4 min by LC-MS analysis and it presented a parent ion peak at $m/z=529$ $[M-H]^-$, which was 162 amu more than that of the substrate (Supporting Information, Figure S6). UDP-

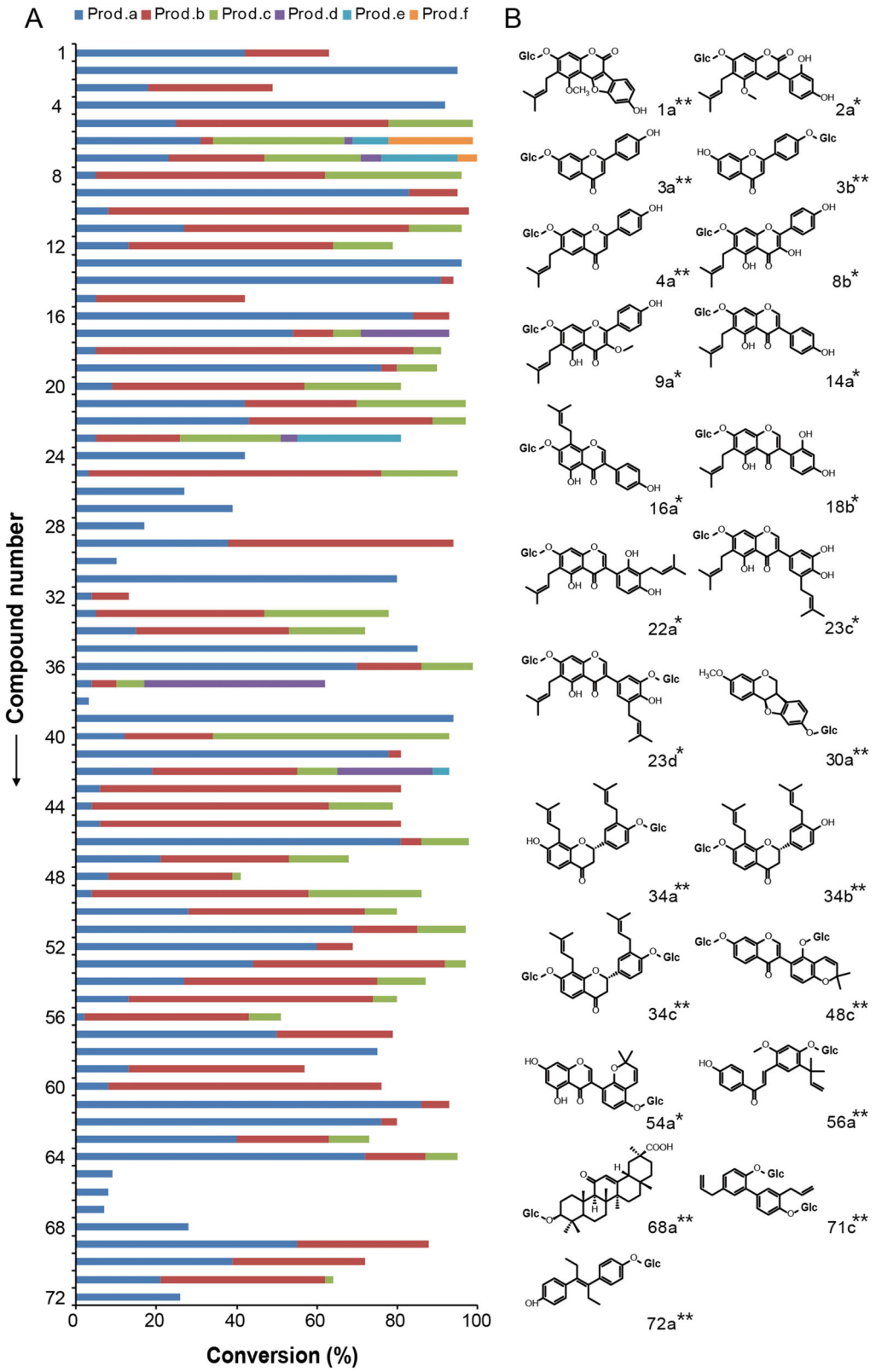

Figure 4. Exploring the substrate promiscuity of MhGT1 with a substrate library. (A) Percent conversions of *O*-glycosylated products catalyzed by MhGT1. The members are listed based on the structural scaffolds shown in part B. The columns with different colours represent the product number and conversion percent. (B) The structures of *O*-glycosylated products catalyzed by MhGT1. The symbol (*) indicates that glycosylated products are identified by comparison with the standards. The symbol (**) indicates that glycosylated products are isolated and elucidated in this study. See the Supporting Information, Figure S4 for a full list of structures.

glucuronic acid and UDP-*N*-acetylglucosamine were not accepted by MhGT1.

Computational Modelling of MhGT1

To understand the broad specificity of MhGT1 to substrate, we built MhGT1 models. Considering that few crystal structures of fungal and yeast GT-B family members have been elucidated and all available structures show very low sequence identities (even less than 12% sequence identity, for example, the *S. cerevisiae* GT (PDB ID: 3zf8) shows 11.6% sequence identity) with our newly identified MhGT1. Thus, traditional template-based homology modelling could not provide satisfactory predictions here. The *de novo* structure predicted method in this study includes both Rosetta[25] *ab initio* and comparative modelling methodology. The *de novo* predicted model by Rosetta reveals a conserved "Rossmann-like" (α/β/α) motif located on the *C*-terminal domain, a truncated *N*-terminal domain, and a long loop creating a natural interdomain cleft (Figure 5A). Docking results exhibit similar binding modes of the UDP-glucose within the donor sugar binding site, which is consistent with the nature of the donor sugar in other GTs described previously.[27] However, although MhGT1 shows a conserved donor site, much more substantial changes in the acceptor site are observed. As shown in Figure 5, it is suggested that the relative truncated sequence in MhGT1 with respect to other GTs would result in a less "Rossmann-like" conformation in the *N*-terminal region. Without the steric hindrance of the twisted β-barrels and the connecting helices in proximity to the cleft, MhGT1 shows a much more open active site architecture compared to GtfA (PDB ID: 1PN3),[26] reflecting the very different nature of the acceptor species. The volume of the active cavity of MhGT1 model monitored by the online sever CASTp[28] (http://sts.bioe.uic.edu/castp/index.php) is 3196 Å3, which is approximately twice as large as those of other GT-B family members (~1500 Å3). Furthermore, a close inspection revealed that the large active cavity of the enzyme contains a mixture of hydrophobic and charged residues, mainly in the form of arginine and aspartic acid, which could recognize variable types of substrates. Taken together, the much larger size of the active cavity and its structural composition

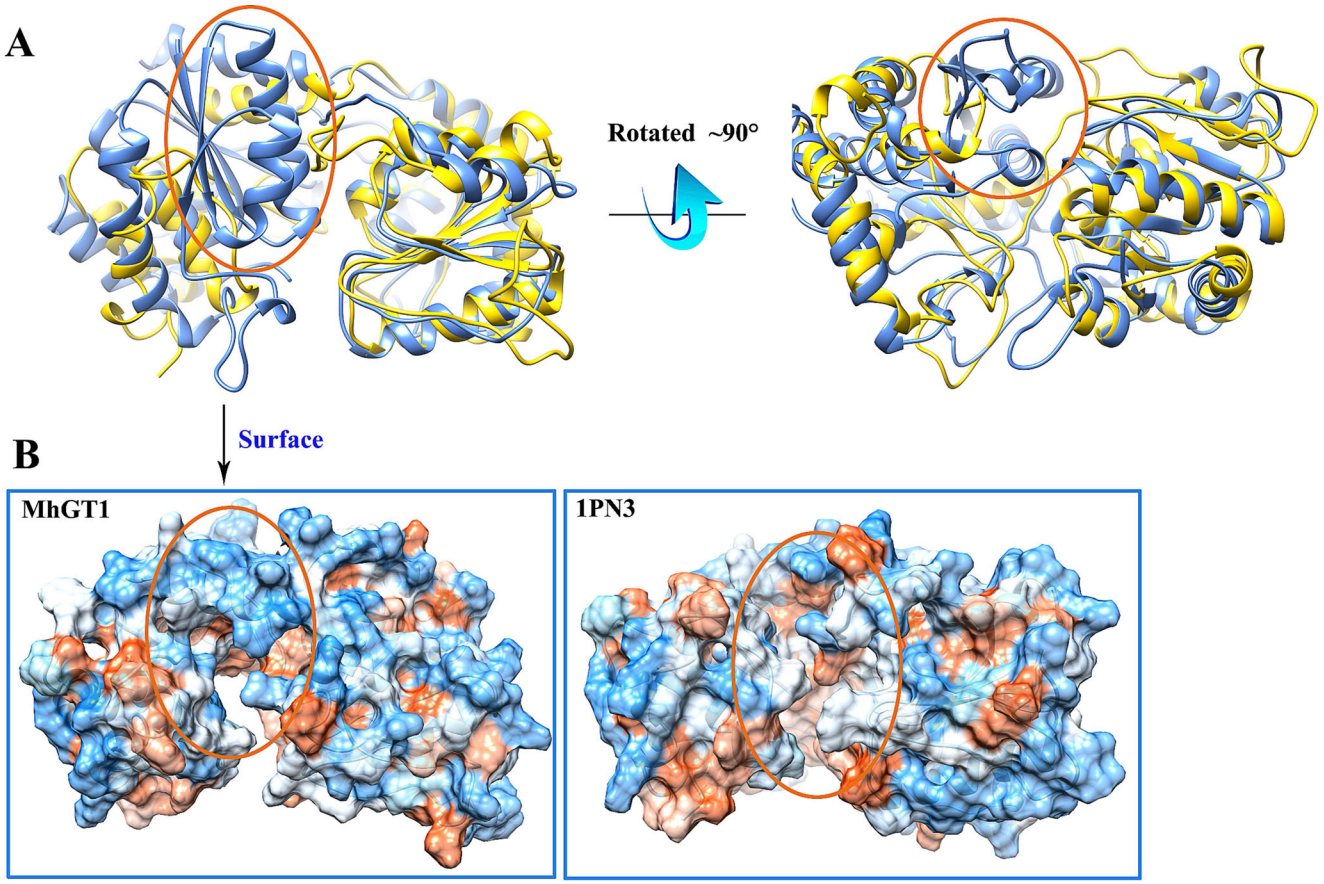

Figure 5. Overall structure of the refined MhGT1 model. (A) Structural comparison between the refined MhGT1 model (yellow) and the crystal structure of GtfA (PDB ID: 1PN3) (blue). (B) Hydrophobic surface representation of the enzymes showing the much more open active site architectures that account for broad substrate scope of MhGT1.

are suggested to account for the broad specificity of MhGT1.

It should be mentioned that 52 members of the library are prenylated compounds (**1**, **2**, **4**, **8**–**14**, **16**–**23**, **25**, **27**, **29**, **31**, **33**–**37**, **39**–**63**) with prenyl residues or moieties derived thereof. High conversion rates of >60% were detected for 48 (except **27**, **48**, **56**, **59**) of these substrates. Small product numbers with such substrates indicated a regiospecificity of MhGT1 towards compounds bearing prenyl moieties. To estimate the impact of prenyl groups on the MhGT1 activity, 6 acceptors (**3**, **5**, **6**, **15**, **24**, **32**) without prenyl groups and the corresponding 12 prenylated derivatives containing one (**4**, **8**–**11**, **14**, **16**, **25**, **33**), two (**12**, **34**) or three prenyl moieties (**35**) were used as substrates for MhGT1 assay (Figure 6 and Supporting Information, Figure S4). The average conversion rate of 89% was calculated for substrates containing prenyl groups, clearly higher than the 55% for that of the substrates without prenyl groups. Furthermore, our results showed that the catalytic activity and efficiency of MhGT1s improved significantly with the prenyl moieties. With the exception for **16**, **25**, and **33**, the substrates with 1 prenyl group showed an average conversion rate of 95%; **12** and **34** containing two prenyl groups exhibited conversion rates of more than 70%, and **35** with 3 prenyl groups showed an absolute conversion rate of 85% with only one product.

To shed some light on the origin of the regiospecificity in the reaction of prenylated phenols, we performed substrate docking and MD simulations (Supporting Information, Figures S7–S9). As shown in Figure S10A (Supporting Information), the walls of the much opening cavity are lined by several hydrophobic residues (V50, I52, W114, I148, F242, F243 and W249) and with an arginine (R24) and two aspartic acid (D46 and D117) residues pointing directly to the cavity. It is suggested that the hydrophobic residues, especially the aromatic residues, are responsible for the position of the prenylated group into the elongated hydrophobic core, making strong non-polar contributions to the binding activity. Thus it is reasonable that the substrates without prenylated groups exhibit decreased binding affinity compared to the prenylated phenols.

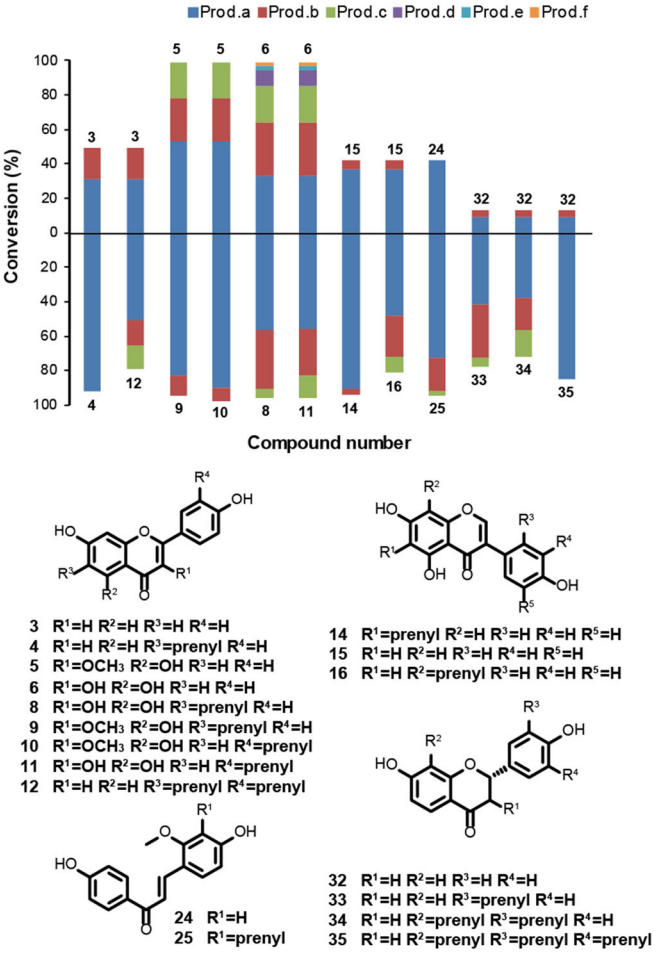

Figure 6. Catalytic regiospecificity of MhGT1 depending on the prenyl moiety in the substrate. Comparison of catalytic efficiency and product number between substrates without prenyl moieties (**3**, **5**, **6**, **15**, **24**, **32**) and with prenyl moieties (**4**, **8**–**12**, **14**, **16**, **25**, **33**–**35**). The different colours represent different glycosylated products. The percent conversion rates of glycosylated products are shown in Table S1 in the Supporting Information.

Structural Elucidation of Glycosylated Compounds and Bioassays

To confirm the glucosylation position and pattern as well as for biological evaluation, 10 mono- (**1a**, **3a**, **3b**, **4a**, **30a**, **34a**, **34b**, **56a**, **68a**, **72a**) and 3 (**34c**, **48c**, **71c**) di-*O*-glucosylated products were isolated on a preparative scale. Their structures were elucidated by HR-ESI-MS, ^{1}H and ^{13}C NMR and HMBC analyses, as described in the Supporting Information (Figures S12–S49). For monoglucoside **1a**, the glucosyl residue exhibited characteristic NMR resonances (the anomeric proton signal at $\delta_H = 5.02$; the anomeric carbon signal at $\delta_C = 100.6$; one CH_2 signal at $\delta_C = 60.7$; and four CH signals at $\delta_C = 69.7$–77.2). For diglucoside **34c**, the glucosyl residue exhibited characteristic NMR resonances (two anomeric proton signals at $\delta_H = 4.83$ and $\delta_H = 4.91$; two anomeric carbon signals at $\delta_C = 100.6$ and $\delta_C = 100.9$; two CH_2 signals at $\delta_C = 60.6$ and $\delta_C = 60.7$; and eight CH signals at $\delta_C = 69.6$–77.2). The coupling constants of the anomeric protons ($J = 7.2$ Hz) suggested the β-glycosidic linkage for all the products. The linkage site for the glucosyl residue was determined by HMBC long-range correlations (see Figures in the Supporting Information). Taking **1a** as an example, the key HMBC cross-peaks from the anomeric proton H-1‴ ($\delta_H = 5.02$) and H-1″ ($\delta_H = 3.36$, 3.53) to

C-7 ($\delta_C = 158.4$) indicated the glucosyl residue was connected to C-7 in **1a**. 10 of them (**1a**, **3a**, **3b**, **4a**, **30a**, **34a–c**, **48c**, **56a**) were found to be novel *O*-glycosides.

As an example, one of the obtained glycosylated products, **1a**, was biologically evaluated for solubility and transportation using the intestinal Caco-2 cell monolayer model.[29] The glycyrol 7-*O*-glucoside's transportation rate is significantly higher than that of glycyrol from apical (AP) to basolateral (BL) side (90–180 min) or BL to AP side (0–180 min) (Supporting Information, Figure S11). This result proved that modification by glycosylation can promote the solubility and absorption of drugs.

Conclusions

In summary, we have discovered and characterized for the first time a phenolic GT MhGT1 from a filamentous fungus and explored its substrate promiscuity. MhGT1 was found to be a new group of GTs and exhibited a robust capability to regio- and stereospecific *O*-glycosylation of 72 structurally diverse drug-like scaffolds and sterols with UDP-glucose as sugar donor (Figure 2C, Figure 4, and Supporting Information, Table S1). Unprecedentedly, MhGT1 showed broad substrate scope and regiospecificy towards prenylated phenols. This was well explained by a computational modelling approach. MhGT1 with a truncated *N*-terminal domain accounts for the broad substrate specificity and the hydrophobic and charged amino acid residues in the MhGT1 active center contribute to the regiospecificy to prenylated substrates. Finally, we created 10 novel glycosylated small molecules including 7 compounds (**1a**, **4a**, **34a–c**, **48c**, **56a**) with both prenyl and glycosyl moieties which are very rare in nature. Our findings shed light on how fungi glycosylate small molecules including natural products, open a new avenue to obtain GTs and expand the enzymatic approach to obtain glycosylated compounds in the drug discovery and development process.

Experimental Section

General

The known compounds **1–6**, **8–34**, **36–39**, **41–59**, **61–63** and **65–68** in the substrate library were isolated from *Glycyrrhiza uralensis*, *G. glabra, G. inflata* and *Bufonis venenum*, respectively.[30] Compounds **7**, **35**, **40**, **60**, **64** and **69–93** were purchased from commercial sources (Solarbio Technology Co. Ltd., Beijing, China). Samples were analyzed on an Agilent 1260 instrument and isolated on an Agilent 1200 instrument (Agilent, Waldbronn, Germany). LC-MS analysis was performed on an LCQ Advantage ion-trap mass spectrometer (Thermo Fisher, CA, USA). NMR spectra were recorded on a Bruker AVANCE III-400 spectrometer (Karlsruhe, Germany) in DMSO-d_6 with TMS as the internal standard. Chemical shifts (δ) are given in parts per million (ppm) and coupling constants (J) are given in Hz.

Microbial Transformation and Product Analysis

Glycyrol (**1**) was fed to *M. hiemalis* for determination of glycosylation rate at the different culture stages (3 h, 6 h, 12 h, 24 h) by using cultures without feeding as a negative control.[31] Then the culture was treated and analyzed on an analytical HPLC with an Agilent Zorbax SB C18 column (250 mm × 4.6 mm, 5 μm) and a flow rate of 1 mL min^{-1}. Extracts of fed cultures were dissolved in methanol, and separated with a linear gradient of acetonitrile in H_2O containing 0.1% formic acid. The compounds of interest were detected within 60 min by using a linear gradient of 15% to 95% acetonitrile in 50 min and a wash step with 100% acetonitrile for 10 min.

RNA Preparation, Sequencing and Assembly

Total RNAs from the mycelia of *M. hiemalis* were extracted by using the Tran*Zol*™ kit (Transgen Biotech, China). The RNAs were controlled in a nucleotide analyzer Quawell Q3000 (Quawell, USA) and reversely transcribed into cDNA with the Fast Quant RT Kit (Tiangen Biotech, China). The RNAs from the control group and the induced group were sequenced by the high-throughput sequencing platform Illumina HiSeqTM2000 (Illumina, USA) to obtain identifiable sequenced reads, namely raw reads.[32] The raw reads were further condensed and simplified to clean reads by evaluating and screening processes. Subsequently, these clean data were merged and assembled by using the software Trinity (http://trinityrnaseq.sourceforge.net/). A library containing clean data was utilized to predict open reading frames (ORF) using the software TransDecoder (https://transdecoder.github.io/) and to translate coding sequences into proteins. Protein encoding genes were annotated through the software Trinotate (http://trinotate.github.io/) based on various bio-database resources. Ultimately, differentially expressed genes were collected as a library for predicting the putative glycosyltransferases through the transcriptome data. However, no target gene was found from this library. To obtain target glycosyltransferases, multiple sequence alignments were performed using the known flavonoid glycosyltransferases BcGT-1, XcGT-2, YjiC, and YjiC1 (Supporting Information, Figure S1).[17,33–35] The candidate protein was targeted from the *M. hiemalis* transcriptome data and named MhGT1 (GenBank Accession Number: KU885980).

Phylogenetic Analysis

Evolutionary analyses of MhGT1 and 26 glycosyltransferases from other species were conducted with MEGA 6.0. The phylogenetic tree was inferred using the Neighbor-Joining method based on ClustalW multiple alignments. Their Genbank accession numbers and organisms are as follows: CaUGT2 (BAD29722.1) from *Catharanthus roseus*;[22] UGT73B2 (EFH43393.1) from *Arabidopsis lyrata* subsp. *lyrata*;[36] UGT73G1 (AAP88406.1) from *Allium cepa*;[37] UGT73AE1 (AJT58578.1) from *Carthamus tinctorius*;[14]

BMGT1 (ACM09993.3) from *Bacopa monnieri*;[38] UGT73A4 (AAS94330.1) from *Beta vulgaris*;[39] GmIF7GT (BAF64416.1) from *Glycine max*;[40] UGT88A4 (ABL85471.1) from *Maclura pomifera*;[41] UF3GaT (BAA36972.1),[42] a galactosyltransferase from *Vigna mungo*; SsBGT1 (XP_001589362.1) from *Sclerotinia sclerotiorum* 1980;[43] OleD (ABA42119.1) from *Streptomyces antibioticus*;[44] BcGT-1 (AAS41089.1) from *Bacillus cereus* ATCC 10987;[17] YjiC (AAU40842.1) from *B. licheniformis* DSM 13;[34] LanGT2 (AAD13553.1) from *S. cyanogenus*;[45] UrdGT2 (AAF00209.1) from *S. fradiae*;[46] SsfS6 (ADE34512.1) from *S.* sp. SF2575;[47] XcGT-2 (AAM41712.1) from *Xanthomonas campestris* pv. *campestris* str. ATCC 33913;[33] UGT52 (AAD28546.1) from *Dictyostelium discoideum*;[19] UGT51 (AAB67475.1) from *Saccharomyces cerevisiae*;[19] UGT51B1 (AAD29570.1) from *Pichia pastoris*;[19] UGT51C1 (AAD29571.1) from *Candida albicans*;[19] UGT53A1 (AAN77909.1) from *Ustilago maydis*; HMPREF1544_00073 (EPB92999.1) from *M. circinelloides* f. *circinelloides* 1006PhL; PFICI_03956 (XP_007830728.1) from *Pestalotiopsis fici* W106-1; PFICI_02610 (XP_007829382.1) from *P. fici* W106-1; PFICI_03732 (XP_007830504.1) from *P. fici* W106-1.

Molecular Cloning, Protein Expression and Purification

The coding region of MhGT1 was amplified from the above cDNA using the designed primers (forward primer: GGC CTT AGC AGG TGC ATG TGG ACG TCC ATG GTA GGT GTA CAT ATG GCT G; reverse primer: GCT TGC CTG CAG GCC ATG GCT AGC CCG TTA TGA GCC TTG ATT TGT TCT TTG C) and inserted into pKLD116 vector (Novagen) according to the Quick-change method to give the plasmid of pYJF14.1.[48] The vector was then introduced into *E. coli* BL21 (DE3) (Transgen Biotech, China). The procedures for protein expression and purification were as described previously.[49] *E. coli* cells were grown in 500 mL LB medium at 37 °C. After OD_{600} reached 0.4–0.6, the cells were induced with 0.5 mM IPTG at 16 °C for 16 h. Then, cell pellets were harvested by centrifugation (6000 rpm, 30 min, 4 °C), and re-suspended in 20 mL lysis buffer (50 mM NaH_2PO_4 pH 8.0, 300 mM NaCl, 10 mM imidazole). After disrupting the cells by sonication on ice, the mixture was centrifuged at 14,000 rpm for 30 min at 4 °C. The supernatant was incubated with Ni-NTA agarose (GE Healthcare) for 2 h at 4 °C. The mixture was loaded onto a pre-equilibrated column and then washed by washing buffer (50 mM NaH_2PO_4 pH 8.0, 300 mM NaCl, 20 mM imidazole). The target protein was eluted by elution buffer containing 250 mM imidazole. The fractions containing target proteins were concentrated to 2.5 mL using a 15 mL Amicon Ultra-50K (Millipore) and desalted with storage buffer (50 mM Tris-HCl, 20% glycerol, pH 7.5). The purified protein was stored at −80 °C.

LC-MS/MS Analysis of MhGT1

The protein band of MhGT1 from SDS-PAGE was cut into 1–2 mm size pieces, then they were tryptically digested at 37 °C overnight for extracting the peptides. The resulting peptide mixture was analyzed by LC-MS/MS as described previously.[50] The peptide mixture (5 μL) was injected at a flow rate of 5 μL min^{-1} onto a pre-column (Easy-column C18-A1,100 μm I.D. × 20 mm, 5 μm, Thermo Fisher Scientific). The chromatographic separation was performed on a reverse-phase C18 column (Easy-column C18-A2, 75 μm I.D. × 100 mm, 3 μm, Thermo Fisher Scientific) at a flow rate of 300 nL/min with a 60 min gradient of 2% to 40% acetonitrile in 0.1% formic acid. The electrospray voltage was maintained at 2.2 kV, and the capillary temperature was set at 250 °C. The LTQ-Orbitrap was operated in data-dependent mode to simultaneously measure full scan MS spectra (m/z = 350–2000) in the Orbitrap with a mass resolution of 60,000 at m/z = 400. After full-scan survey, the 15 most abundant ions detected in the full-MS scan were measured in the LTQ part by collision-induced dissociation (CID), respectively. Each sample was analyzed in triplicate.

Biochemical Characterization of MhGT1

For characterizing MhGT1, the glycosylation reaction was performed in a final volume of 100 μL containing 50 mM Tris-HCl (pH 8.0), 25 μM aglycone, 250 μM UDP-glucose, 50 μg of purified enzyme and 5 mM $CaCl_2$. The reaction mixtures were incubated at 37 °C for 4 h and terminated by adding 100 μL of MeOH. The protein was removed by centrifugation at 12,000 rpm for 10 min. Then supernatants were analyzed by HPLC and LC-MS. The enzymatic products were separated with a linear gradient of 20 to 100% methanol in H_2O containing 0.1% formic acid in 20 min, followed by 100% MeOH for 5 min. The total conversion yield in percent was calculated using a method of peak area integration.

Effects of pH, Temperature and Divalent Metal Ions

To test the optional pH value for MhGT1 activity, assays were performed in different reaction buffers ranged in pH values from 4.0–6.0 (citric acid-sodium citrate buffer) and 7.0–11.0 (Tris-HCl buffer). To study the optional reaction temperature for MhGT1 activity, different temperatures from 4–60 °C were investigated. To determine the dependence of MhGT1 activities on metal ions, reactions were carried out in the presence of different salts such as $CaCl_2$, $MgCl_2$, $BaCl_2$, $MnCl_2$, $CoCl_2$, $FeCl_2$, $CuCl_2$, and $ZnCl_2$ at a final concentration of 5 mM. The reaction with 5 mM EDTA was set as control. All reactions were conducted with UDP-glucose as a donor and glycycoumarin as an acceptor. Each value represents mean value of three parallel measurements, and all reactions were terminated with MeOH and centrifuged at 12,000 rpm for 10 min for next HPLC analysis as described above.

Kinetic Studies

For determination of the kinetic parameters of various substrates, assays were performed in a final volume of 100 μL, consisting of 50 mM Tris-HCl (pH 8.0), 20 μg of MhGT1, 500 μM of saturating UDP-glucose, and varying concentrations (0, 5, 7.5, 10, 20, 40 μM) of glycycoumarin (**2**), licoflavone A (**4**), licoarylcoumarin (**13**), and wighteone (**14**). The reactions were quenched with 100 μL MeOH and centrifuged at 12,000 rpm for 10 min. The enzymatic products were analyzed with a reversed-phase HPLC column as described above. All experiments were performed in triplicate.

The K_m value was calculated by using the Lineweaver–Burk plot method.

Enzyme Assays of MhGT1

To explore the aglycone promiscuity and specificity of MhGT1, diverse acceptors were tested, including flavonoids, coumarins, coumarones, anthraquinones, alkaloids, glucosides, terpenoids, steroids, antibiotics, lignans, tanshinone, amino acids, and other phenolic compounds. All reactions were individually conducted in a final volume of 100 μL buffer containing 50 mM Tris-HCl (pH 8.0), 25 μM aglycone, 250 μM UDP-glucose, 50 μg of purified enzyme and 5 mM $CaCl_2$. Reactions were incubated at 37 °C for 4 h and terminated by adding 100 μL MeOH. After centrifugation at 12,000 rpm for 10 min, the supernatants were collected for analysis by HPLC and LC-MS. To study the tolerance of MhGT1 for other UDP-sugars, glycosylation reactions with UDP-galactose, UDP-glucuronic acid, and UDP-*N*-acetylglucosamine were conducted by using glycycoumarin (**2**) as an acceptor. The reaction was performed in a final volume of 100 μL containing 40 μg purified enzyme and was incubated at 37 °C for 12 h. Aliquots were analyzed on a reversed-phase HPLC and LC-MS as described above.

Preparative-Scale Reactions

The crude enzyme of MhGT1 was extracted from 500 mL of *E. coli* culture induced by IPTG and stabilized in 20 mL of reaction buffer (50 mM Tris-HCl, pH 8.0) with 20 μmol of aglycone dissolved in 1 mL DMSO and 50 μmol of UDP-glucose. The reactions were incubated at 37 °C for 6 h and the products were extracted 2 times with ethyl acetate. The organic phase was concentrated and dissolved in 1 mL MeOH. The glycosylated products were separated on a reverse-phase semi-preparative HPLC and characterized by LC-MS, ^{1}H and ^{13}C NMR.

Computational Modelling

Models for MhGT1 were built by the Rosetta[25] *ab initio* and comparative modelling methodology. The initial step, called "Ginzu", involves screening the query sequence for regions that possess a homologue with an experimentally characterized structure with BLAST, PSI-BLAST, and FFAS03 and 3D-Jury, followed by cutting the sequence into putative domains based on matches to known families and structures, multiple sequence information, and predicted secondary structure information. Then the detected parents and the regions of the query are stored and assigned to the template-based modelling protocol with multiple sequence alignment (MSA) based methods. Once the chain is completely assembled, the side-chains of the final models are repacked using a Monte Carlo algorithm. GtfA protein and MhGT1 are both involved in the GT-B glycosyltransferases family. The Ginzu domain prediction module by Rosetta reveals that GtfA shows the highest sequence identity (20.5% sequence identity) among all available structures. In addition, the crystal structure of GtfA also contains a UDP-glucose-like ligand, TDP, within the donor sugar binding site. Therefore, GtfA was used as a reference to choose the MhGT1 model among all obtained models predicted by Rosetta. The fragment files were generated using the Robetta online server (http://robetta.bakerlab.org/). The whole process contains two procedures and ends up with a rebuild-and-refinement protocol. The first protocol uses a reduced force field to describe interatomic interactions. In this protocol, the protein is separated to several regions and constructed utilizing fragment libraries. Then the program employs a full-atom model, and a minimization of the potential energy is performed using a *Monte Carlo* algorithm. The resulting 300 refined models were sorted by RMSD values with respect to the reference protein GtfA (PDB ID: 1PN3).[26] Then the top scoring model was refined by MD simulation.

Molecular Dynamics (MD) Simulations

MD simulations were performed using AMBER 12 software package[51] and the ff12SB force field. To keep the whole systems neutral, chloride ions (Cl^-) were added based on a coulomb potential grid. Each system was then solvated with the TIP3P water model in a truncated octahedron box with a 10 Å distance around the solute. Then 2000 steps of steepest decent minimization and 3000 steps of conjugate gradient minimization were performed. The systems were subsequently heated from 0 K to 300 K in 300 ps by a Langevin dynamics followed by 500 ps equilibrium MD simulations. Finally, a total of 10 ns was simulated under NPT ensemble conditions using periodic boundary conditions and particle-mesh Ewald (PME) for long-range electrostatics. The time step was set to 2 fs. The structural optimizations of ligand molecules were conducted using B3LYP combined with 6–31+G* basis set using the *Gaussian 09* software.[52] RESP fitting procedure was used for charge derivation based on the optimal conformation. Finally, the force field parameters of each substrate were derived using the antechamber module of AMBER 12.

Molecular Docking

Autodock 4.2[53] was used to dock UDP-glucose and the sugar acceptor substrates into the MhGT1 model. We first docked the UDP-glucose into the MhGT1 model, and chose the top ranked binding pose with lowest binding energy among the 100 poses. After 15 ns MD simulation of the MhGT1/UDP-glucose complex, the sugar acceptor substrates were subsequently docked into the representative complex structure of the trajectory. Autodock cluster analysis was performed of the collected conformations based on the RMSD value using the conformation with the lowest-binding energy as the reference. The docking results were carefully examined based on the binding energies as well as the stereo-chemical relevance. After docking, we applied 10 ns MD simulations for each MhGT1/UDP-glucose/substrate complex and generated the representative triplex complex structures from the trajectories by cluster analysis.

Bidirectional Transport Experiments

Bidirectional transport experiments of glycyrol (**1**) and glycyrol 7-*O*-glucoside (**1a**) have been described previously.[54] Caco-2 cell monolayer was washed three times with HBSS and incubated in fresh HBSS for 30 min at 37 °C. Pure compound solutions (10 μM) were added to either the apical (AP, 0.5 mL) or basolateral side (BL, 1.5 mL). The cells

were incubated in an orbital shaker at 37 °C, 50 r/min. 0.3 mL of aliquot of sample were removed to measure the transport rate at 30, 60, 90, 120, 150, and 180 min, and the remaining sample was immediately replenished with an equal volume of HBSS. The samples were freeze-dried, redissolved, filtered and analyzed by LC-MS. All experiments were repeated in triplicate. The transportation rate was calculated as the ratio of cumulative concentration in the receiver to the donor side × 100%.

Acknowledgements

This work was supported by National Key Research and Development Program (2016YFD0400105) and the National Natural Science Foundation of China (Grant No 81222054). W.B.Y. is a scholar of "the 100 Talents Project" of CAS.We thank Dr. Istvan Molnar (University of Arizona) for the critical reading and helpful discussions.

References

[1] H. S. Lee, J. S. Thorson, *Anal. Biochem.* **2011**, *418*, 85–88.
[2] G. J. Williams, C. Zhang, J. S. Thorson, *Nat. Chem. Biol.* **2007**, *3*, 657–662.
[3] C. J. Thibodeaux, C. E. Melancon, H. W. Liu, *Nature* **2007**, *446*, 1008–1016.
[4] M. M. Palcic, *Curr. Opin. Chem. Biol.* **2011**, *15*, 226–233.
[5] F. De Bruyn, J. Maertens, J. Beauprez, W. Soetaert, M. De Mey, *Biotechnol. Adv.* **2015**, *33*, 288–302.
[6] H. Cao, X. Chen, A. R. Jassbi, J. Xiao, *Biotechnol. Adv.* **2015**, *33*, 214–223.
[7] J. Xiao, T. S. Muzashvili, M. I. Georgiev, *Biotechnol. Adv.* **2014**, *32*, 1145–1156.
[8] A. Bartmanska, T. Tronina, E. Huszcza, *Bioorg. Med. Chem. Lett.* **2012**, *22*, 6451–6453.
[9] E. A. Abourashed, J. R. Mikell, I. A. Khan, *Bioorg. Med. Chem.* **2012**, *20*, 2784–2788.
[10] R. W. Gantt, P. Peltier-Pain, S. Singh, M. Zhou, J. S. Thorson, *Proc. Natl. Acad. Sci. USA* **2013**, *110*, 7648–7653.
[11] M. Weis, E. K. Lim, N. Bruce, D. Bowles, *Angew. Chem.* **2006**, *118*, 3614–3618; *Angew. Chem. Int. Ed.* **2006**, *45*, 3534–3538.
[12] G. J. Williams, R. W. Gantt, J. S. Thorson, *Curr. Opin. Chem. Biol.* **2008**, *12*, 556–564.
[13] S. Singh, G. N. Phillips Jr, J. S. Thorson, *Nat. Prod. Rep.* **2012**, *29*, 1201–1237.
[14] K. Xie, R. Chen, J. Li, R. Wang, D. Chen, X. Dou, J. Dai, *Org. Lett.* **2014**, *16*, 4874–4877.
[15] D. Chen, R. Chen, R. Wang, J. Li, K. Xie, C. Bian, L. Sun, X. Zhang, J. Liu, L. Yang, F. Ye, X. Yu, J. Dai, *Angew. Chem.* **2015**, *127*, 12869–12873; *Angew. Chem. Int. Ed.* **2015**, *54*, 12678–12682.
[16] S. Ji, W.-F. Liang, Z.-W. Li, J. Feng, Q. Wang, X. Qiao, M. Ye, *RSC Adv.* **2016**, *6*, 20791–20799.
[17] J. H. Ko, B. G. Kim, A. Joong-Hoon, *FEMS Microbiol. Lett.* **2006**, *258*, 263–268.
[18] K. R. Reiding, D. Blank, D. M. Kuijper, A. M. Deelder, M. Wuhrer, *Anal. Chem.* **2014**, *86*, 5784–5793.
[19] D. Warnecke, R. Erdmann, A. Fahl, B. Hube, F. Muller, T. Zank, U. Zahringer, E. Heinz, *J. Biol. Chem.* **1999**, *274*, 13048–13059.
[20] C. T. Walsh, H. C. Losey, C. L. Freel Meyers, *Biochem. Soc. Trans.* **2003**, *31*, 487–492.
[21] B. Hofer, *Appl. Microbiol. Biotechnol.* **2016**, *100*, 4269–4281.
[22] Y. Kaminaga, F. P. Sahin, H. Mizukami, *FEBS Lett.* **2004**, *567*, 197–202.
[23] R. W. Gantt, R. D. Goff, G. J. Williams, J. S. Thorson, *Angew. Chem.* **2008**, *120*, 9021–9024; *Angew. Chem. Int. Ed.* **2008**, *47*, 8889–8892.
[24] R. P. Pandey, R. B. Gurung, P. Parajuli, N. Koirala, T. Tuoile, J. K. Sohng, *Carbohydr. Res.* **2014**, *393*, 26–31.
[25] D. E. Kim, D. Chivian, D. Baker, *Nucleic Acids Res.* **2004**, *32*, W526–531.
[26] A. M. Mulichak, H. C. Losey, W. Lu, Z. Wawrzak, C. T. Walsh, R. M. Garavito, *Proc. Natl. Acad. Sci. USA* **2003**, *100*, 9238–9243.
[27] D. Albesa-Jove, D. Giganti, M. Jackson, P. M. Alzari, M. E. Guerin, *Glycobiology* **2014**, *24*, 108–124.
[28] J. Dundas, Z. Ouyang, J. Tseng, A. Binkowski, Y. Turpaz, J. Liang, *Nucleic Acids Res.* **2006**, *34*, W116–118.
[29] P. Artursson, K. Palm, K. Luthman, *Adv. Drug Delivery Rev.* **2001**, *46*, 27–43.
[30] S. Ji, Z. Li, W. Song, Y. Wang, W. Liang, K. Li, S. Tang, Q. Wang, X. Qiao, D. Zhou, S. Yu, M. Ye, *J. Nat. Prod.* **2016**, *79*, 281–292.
[31] J. Feng, W. Liang, S. Ji, X. Qiao, Y. Zhang, S. Yu, M. Ye, *J. Chin. Pharm. Sci.* **2015**, *24*, 285–291.
[32] Y. Zhang, G. Luo, D. Liu, D. Wang, W. Yang, J. Sun, A. Zhang, K. Zhan, *PLoS One* **2015**, *10*, e0131559.
[33] H. J. Kim, B. G. Kim, J. A. Kim, Y. Park, Y. J. Lee, Y. Lim, J. H. Ahn, *J. Microbiol. Biotechnol.* **2007**, *17*, 539–542.
[34] C. Z. Wu, J. H. Jang, M. Woo, J. S. Ahn, J. S. Kim, Y. S. Hong, *Appl. Environ. Microbiol.* **2012**, *78*, 7680–7686.
[35] S. L. Luo, L. Z. Dang, K. Q. Zhang, L. M. Liang, G. H. Li, *Lett. Appl. Microbiol.* **2015**, *60*, 72–78.
[36] M. G. Willits, M. t. Giovanni, R. T. N. Prata, C. M. Kramer, V. De Luca, J. C. Steffens, G. Graser, *Phytochemistry* **2004**, *65*, 31–41.
[37] C. M. Kramer, R. T. N. Prata, M. G. Willits, V. De Luca, J. C. Steffens, G. Graser, *Phytochemistry* **2003**, *64*, 1069–1076.
[38] Ruby, R. J. Santosh Kumar, R. K. Vishwakarma, S. Singh, B. M. Khan, *Mol. Biol. Rep.* **2014**, *41*, 4675–4688.
[39] J. Isayenkova, V. Wray, M. Nimtz, D. Strack, T. Vogt, *Phytochemistry* **2006**, *67*, 1598–1612.
[40] A. Noguchi, A. Saito, Y. Homma, M. Nakao, N. Sasaki, T. Nishino, S. Takahashi, T. Nakayama, *J. Biol. Chem.* **2007**, *282*, 23581–23590.
[41] L. Tian, J. W. Blount, R. A. Dixon, *FEBS Lett.* **2006**, *580*, 6915–6920.
[42] M. Mato, Y. Ozeki, Y. Itoh, D. Higeta, K. Yoshitama, S. Teramoto, R. Aida, N. Ishikura, M. Shibata, *Plant Cell Physiol.* **1998**, *39*, 1145–1155.
[43] A. C. Sexton, Z. Minic, A. J. Cozijnsen, M. S. Pedras, B. J. Howlett, *Fungal Genet. Biol.* **2009**, *46*, 201–209.

[44] M. Yang, M. R. Proctor, D. N. Bolam, J. C. Errey, R. A. Field, H. J. Gilbert, B. G. Davis, *J. Am. Chem. Soc.* **2005**, *127*, 9336–9337.
[45] A. Luzhetskyy, T. Taguchi, M. Fedoryshyn, C. Durr, S. E. Wohlert, V. Novikov, A. Bechthold, *ChemBioChem* **2005**, *6*, 1406–1410.
[46] B. Faust, D. Hoffmeister, G. Weitnauer, L. Westrich, S. Haag, P. Schneider, H. Decker, E. Kunzel, J. Rohr, A. Bechthold, *Microbiology* **2000**, *146, (Pt 1)* 147–154.
[47] L. B. Pickens, W. Kim, P. Wang, H. Zhou, K. Watanabe, S. Gomi, Y. Tang, *J. Am. Chem. Soc.* **2009**, *131*, 17677–17689.
[48] J. W. Bok, N. P. Keller, *Methods Mol. Biol.* **2012**, *944*, 163–174.
[49] R. A. Cacho, W. Jiang, Y. H. Chooi, C. T. Walsh, Y. Tang, *J. Am. Chem. Soc.* **2012**, *134*, 16781–16790.
[50] B. Hessling, F. Bonn, A. Otto, F. A. Herbst, G. M. Rappen, J. Bernhardt, M. Hecker, D. Becher, *Int. J. Med. Microbiol.* **2013**, *303*, 624–634.
[51] D. Case, T. Darden, T. Cheatham III, C. Simmerling, J. Wang, R. Duke, R. Luo, R. Walker, W. Zhang, K. Merz, *AMBER 11*, University of California, San Francisco, **2010**.
[52] M. Frisch, H. GWT, G. Schlegel, M. Scuseria, J. Robb, G. S. Cheeseman, V. Barone, B. Mennucci, G. Petersson, H. Nakatsuji, *Gaussian 09*. Gaussian, Inc., Wallingford, **2009**.
[53] G. M. Morris, R. Huey, W. Lindstrom, M. F. Sanner, R. K. Belew, D. S. Goodsell, A. J. Olson, *J. Comput. Chem.* **2009**, *30*, 2785–2791.
[54] Q. Wang, X. Qiao, Y. Qian, Z. Li, Y. Tzeng, D. Zhou, D. Guo, M. Ye, *Nat. Prod. Bioprospect.* **2015**, *5*, 237–246.

Regio- and Stereospecific *O*-Glycosylation of Phenolic Compounds Catalyzed by a Fungal Glycosyltransferase from *Mucor hiemalis*

Adv. Synth. Catal. **2017**, *359*, 1 – 13

Jin Feng, Peng Zhang, Yinglu Cui, Kai Li, Xue Qiao, Ying-Tao Zhang, Shu-Ming Li, Russell J. Cox, Bian Wu, Min Ye,* Wen-Bing Yin*